Available online at www.sciencedirect.com
ScienceDirect
Journal of Power Sources 162 (2006) 1275–1281
JOURNAL OF POWER SOURCES
www.elsevier.com/locate/jpowsour

Carbon nanotubes (CNTs) as a buffer layer in silicon/CNTs composite electrodes for lithium secondary batteries

Taeahn Kim [a], Y.H. Mo [b], K.S. Nahm [b], Seung M. Oh [a,*]

[a] *School of Chemical and Biological Engineering, and Research Center for Energy Conversion & Storage, Seoul National University, Seoul 151-744, South Korea*
[b] *School of Chemical Engineering and Technology, Chonbuk National University, Chonju 561-756, South Korea*

Received 3 April 2006; accepted 21 July 2006
Available online 20 September 2006

Abstract

A core/shell type silicon/carbon nanotubes (Si/CNTs) composite is prepared and its anodic performance in lithium secondary batteries is examined. For the growth of CNTs, a Ni catalyst is loaded on a Si surface by electroless deposition. The growth is performed by chemical vapour deposition at 600 °C using C_2H_2/H_2 but is successful only on smaller and thinner Ni deposits. This is probably due to an easier transformation to small droplets that initiate the growth reaction. The anodic performance of a Si/CNTs composite electrode is superior to that observed with bare Si and Si/CNTs mixed electrodes. This beneficial feature is ascribed to the conductive buffering role of the CNTs layer. It is likely that the void space and the flexible characteristics in the CNTs buffer layer on the Si surface allow volume expansion of the Si core without severe electrode swelling. Because of this, the electric conductive network made among Si particles, carbon network and current-collector is well maintained, which reduces the charge-transfer resistance.

Keywords: Lithium secondary batteries; Silicon negative electrode; Carbon nanotubes; Chemical vapour deposition; Electroless deposition; Conductive buffering

1. Introduction

Recently, considerable attention has been paid to Li-alloy materials such as Si, Al and Sn for the negative electrode of lithium secondary batteries because they possess a higher theoretical specific capacity than that of graphite [1–4]. Among these, Si has the highest value. The practical use of Si powder is, however, still hindered because of two major problems. One is the low electrical conductivity and the other is the severe volume expansion/contraction during the alloying and de-alloying reaction with Li^+ ions [5–8]. The failure modes in Si power electrodes have been identified in previous studies [9,10]. It was found [10] that Si particles expand upon charging as a result of the alloying reaction. This led to swelling of the electrode layer, where carbon powder is also added to compensate for the poor conductivity of Si particles. In the following discharge period, the Si particles contracted as a result of the de-alloying reaction, but the electrode layer still remained swollen because the electrode layer was not elastic. The net result after charge–discharge cycling was a breakdown of the conductive network made between Si, carbon particles and the current-collector.

Several approaches have been made to solve these problems. For instance, breakdown of the conductive network can be minimized either by applying a pressure on cells [10] using an elastomeric binder [11], or composite formation with conductive materials such as carbon [12,13]. We have proposed another approach, wherein CNTs are utilized as a buffering conductive layer in a core/shell type Si/CNTs composite material [14]. During the preparation of this manuscript, related work has just been reported by Shu et al. in their short communication [15], wherein a performance improvement of Si negative electrode has been ascribed to the maintenance of conductive network and the formation of stable solid electrolyte interface (SEI) on CNTs surface. In this paper, we present an enhanced view, particularly on the catalyst size effect on CNTs growth and the role of CNTs in core/shell type Si/CNTs composite material, which is deeply associated with the presence of a large amount of void space within the CNTs shell layer and the mechanical flexibil-

* Corresponding author. Tel.: +82 2 880 7074; fax: +82 2 872 5755.
E-mail address: seungoh@plaza.snu.ac.kr (S.M. Oh).

0378-7753/$ – see front matter © 2006 Elsevier B.V. All rights reserved.
doi:10.1016/j.jpowsour.2006.07.062

ity of CNTs. To address the advantageous features provided by this composite, the evolution of internal resistance upon cycling is monitored by a.c. impedance measurements. The results are compared with those for bare Si and Si/CNTs mixed electrodes.

2. Experimental

2.1. Materials

The composite materials were prepared *via* two consecutive steps, namely, an electroless Ni deposition on Si powder, followed by a chemical vapour deposition (CVD) of CNTs. The Ni deposits were utilized as a catalyst for CNTs growth. For Ni deposition, Si powder (High Purity Chemicals Co., 5 μm, 98%) was first activated by suspension for 30 min in a stirred solution containing 0.1 wt.% $PdCl_2$ in dilute HCl [16]. The electroless Ni deposition was carried out in a plating bath, which had the composition shown in Table 1. $NiSO_4{\cdot}6H_2O$ was used as the Ni source, $NaH_2PO_4{\cdot}H_2O$ as the reducing agent, $(NH_4)_2SO_4$ as the buffering agent, and sodium citrate as the complexing agent. The detailed role of each ingredient can be referenced in the literature [17,18]. In practice, the plating bath was warmed at 80 °C with stirring, into which the activated Si powder was poured. After 5 s the bath was rapidly cooled to 25 °C and stirred for an additional 1 h to allow the growth of Ni deposits. The CNTs were grown over the Ni-deposited Si powder at 600 °C for 30 min by introducing a mixture of C_2H_2/H_2 into a CVD reactor at a flow rate of 10/100 sccm. The reactor pressure was maintained at 1 Torr.

Microscopic investigations were carried out with a JEOL JEM 2000 EXII transmission electron microscope (TEM) and a JEOL JSM-6700F scanning electron microscope (SEM). The Ni content in the Ni-deposited Si powder was analyzed by the inductively-coupled plasma (ICP-AES, Shimadzu, ICP-1000IV) technique. For this, the Ni-deposited Si powder was dissolved with concentrated HNO_3 and the Ni-containing solution was separated from the undissolved Si residue by centrifugation. The carbon contents in Si/CNTs composites were determined from thermogravimetric analysis (TGA) profiles that were recorded from room temperature to 1000 °C at 10 °C min^{-1} in air with a TA instrument Q600 simultaneous DSC/TGA analyzer.

2.2. Electrochemical characterization

To prepare the negative electrodes, a mixture of the Si/CNTs composite powder (or Si powder alone, or a physical mixture), Super P (as a carbon additive for conductivity enhancement) and polyvinylidene fluoride (PVdF, as a polymeric binder) in a 8:1:1 weight ratio was dispersed in *N*-methyl pyrrolidone (NMP) and homogenized. The resulting slurry was spread on a piece of copper foil (thickness = 25 μm and apparent area = 1 cm^2) and dried in vacuum at 120 °C for 12 h. It was then pressed to enhance the inter-particle contact and to ensure a better adhesion to the current-collector. A beaker-type, three-electrode cell was employed to assess the electrochemical performance of the samples. Lithium foils (Cyprus Co.) were used as the counter and the reference electrodes, and 1.0 M $LiClO_4$ dissolved in a mixture of ethylene carbonate (EC) and diethyl carbonate (DEC) (1:1, v/v) was used as the electrolyte. Galvanostatic charge–discharge cycling was conducted at a current density of 100 mA g^{-1} in the voltage range of 0.0–2.0 V (versus Li^+/Li). Electrochemical impedance spectroscopy (EIS) was performed using an Advanced Electrochemical Work Station (CH Instruments, CH660A). The measurements were made in a frequency range from 100 kHz to 10 mHz with an a.c. amplitude of 5 mV and the data analysis was undertaken with Zview software (Scribner Associates Inc.).

Table 1
Composition of nickel electroless plating bath and deposition condition

Chemical	Composition (mol l^{-1})
$NiSO_4{\cdot}6H_2O$	0.1
$NaH_2PO_4{\cdot}H_2O$	0.15
$(NH_4)_2SO_4$	0.5
Sodium citrate	0.2
Temperature (°C)	25
Deposition time (h)	1
pH (adjusted with NH_4OH)	8.0

3. Results and discussion

3.1. Preparation and characterization of Si/CNTs composites

Fig. 1(a) compares the SEM image of bare Si surface (left panel) with that of the Ni-deposited Si surface (right panel) that was obtained by electroless deposition under the conditions given in Table 1. The bare Si particles show clean surfaces in contrast to the roughened surfaces (the lighter dot-like image on the right) of the Ni-deposited Si particles. A magnified view clearly shows the presence of Ni deposits that carry two different morphologies (Fig. 1(b)). One is spherical grains of several tens of nanometers in diameter and the other is smaller grains that are densely deposited to give a film-like external view (indicated as a circle). Takano et al. [16] studied the mechanism of electroless Ni deposition on a Si surface. According to their findings, Ni deposition on a Si proceeds by two routes: (i) Ni(II) reduction by a reducing agent such as NaH_2PO_4 and (ii) a galvanic displacement reaction. The former is the faster process so as to generate larger Ni deposits. The latter, which is the Ni(II) reduction by the electrons released by electrochemical oxidation of Si, is the slower process such that the Ni deposits are smaller and sometimes have the appearance of a thin film [18]. Based on that investigation, the formation mechanism for two types of Ni deposits in this work can be addressed. That is, it is likely that the spherical grains are nucleated and grown by the reducing agent, whereas the smaller film-like deposits are formed by the galvanic displacement reaction. Note that the electroless deposition condition in this work is comparable with that employed by Takano et al [16].

Fig. 1(c) displays the SEM image of Ni deposits that were prepared under different conditions, namely, nucleation and growth at 80 °C for 2 h. The deposition temperature is higher and deposition time is longer than those for Fig. 1(b). As

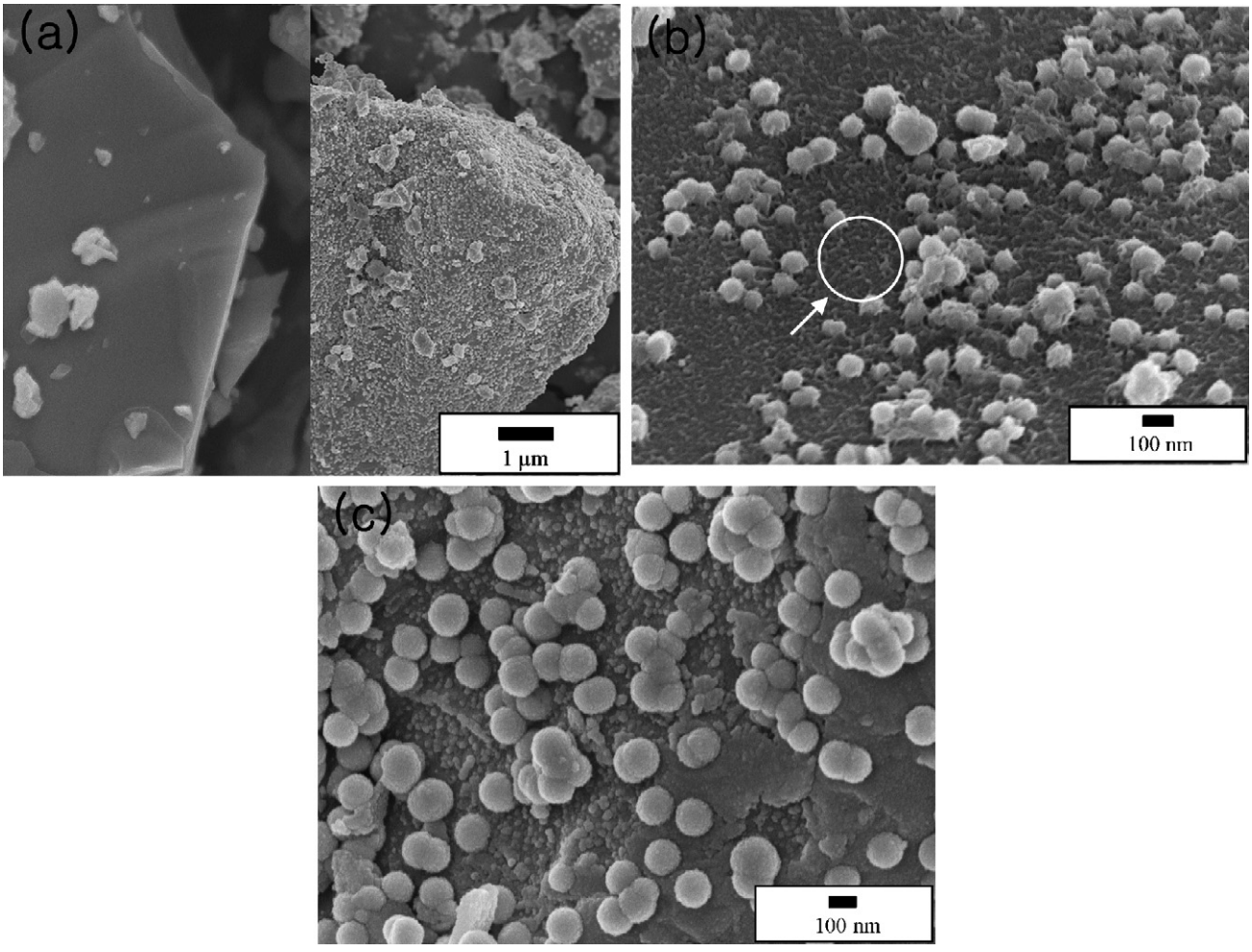

Fig. 1. (a) SEM image of bare Si surface (left panel) and Ni-deposited Si surface (right panel) obtained by electroless deposition under conditions provided in Table 1. (b) Magnified view of Ni-deposited Si surface. Note presence of two types of Ni deposits. (c) SEM image of Ni deposits prepared at 80 °C for 2 h.

expected, both of two types of deposits are grown up to >100 nm and >10 nm, respectively. Some of the latter deposits become a thick film.

The SEM images of CNTs that were grown on the Ni-deposited Si particles at 600 °C for 5 and 30 min are presented in Fig. 2(a) and (b), respectively. Note that this Ni-deposited Si powder was prepared according to the conditions listed in Table 1. The sample grown for 5 min shows the presence of coiled CNTs that have diameters of less than 10 nm (Fig. 2(a)). CNTs of larger size (ca. 100 nm in diameter) appear only in the sample grown for 30 min (Fig. 2(b)). This illustrates that the growth takes place preferentially on the smaller Ni particles [19]. It is well known that the diameter of CNTs is determined by the size of the catalytic metal particles [20,21]. The two different types of CNTs in Fig. 2(b) can thus be assigned to being formed on two different Ni catalysts. It is very likely that the thicker CNTs (ca. 100 nm in diameter in Fig. 2(b)) are grown on the larger Ni deposits (spherical grains of ca. 100 nm in Fig. 1(b)), and the thinner ones on the smaller Ni catalysts. The latter can be confirmed in Fig. 2(c), where it is clearly seen that Ni catalyst particles of ca. 10 nm in diameter are lifted to the top of the same-sized CNTs (indicated as a circle). In addition to the size match between the catalyst particles and CNTs, the SEM image in Fig. 2(c) illustrates that the tip growth mode, among others, is prevailing in this system, which may be due to a weak adhesion between Ni and Si [22].

Fig. 2(d) shows the SEM image of the CNTs that were grown on the Ni-deposited Si particles whose morphology is shown in Fig. 1(c). Note that the CNTs growth is the same as for Fig. 2(a) and (b), but that the size of Ni deposits is larger in this sample. As seen, the deposited Ni particles are melted down and CNTs growth is unsuccessful. It is generally accepted that the initiation of CNTs growth on Ni catalyst is possible when either initially continuous film-like Ni deposits or initially large Ni particles are broken into droplets that are smaller than the critical size that is dependent on the growth parameters [19]. The unsuccessful growth on the heavily-deposited Ni catalysts may thus be ascribed to an unsuccessful formation of smaller Ni droplets. It is apparent that the Ni deposits are agglomerated and melted down, instead of being transformed to droplets, because they are too thick and too large. In the case of a successfully grown sample, small Ni droplets are generated to initiate the growth reaction and reside on top of the CNTs to provide the catalytic sites for continued CNTs growth [19].

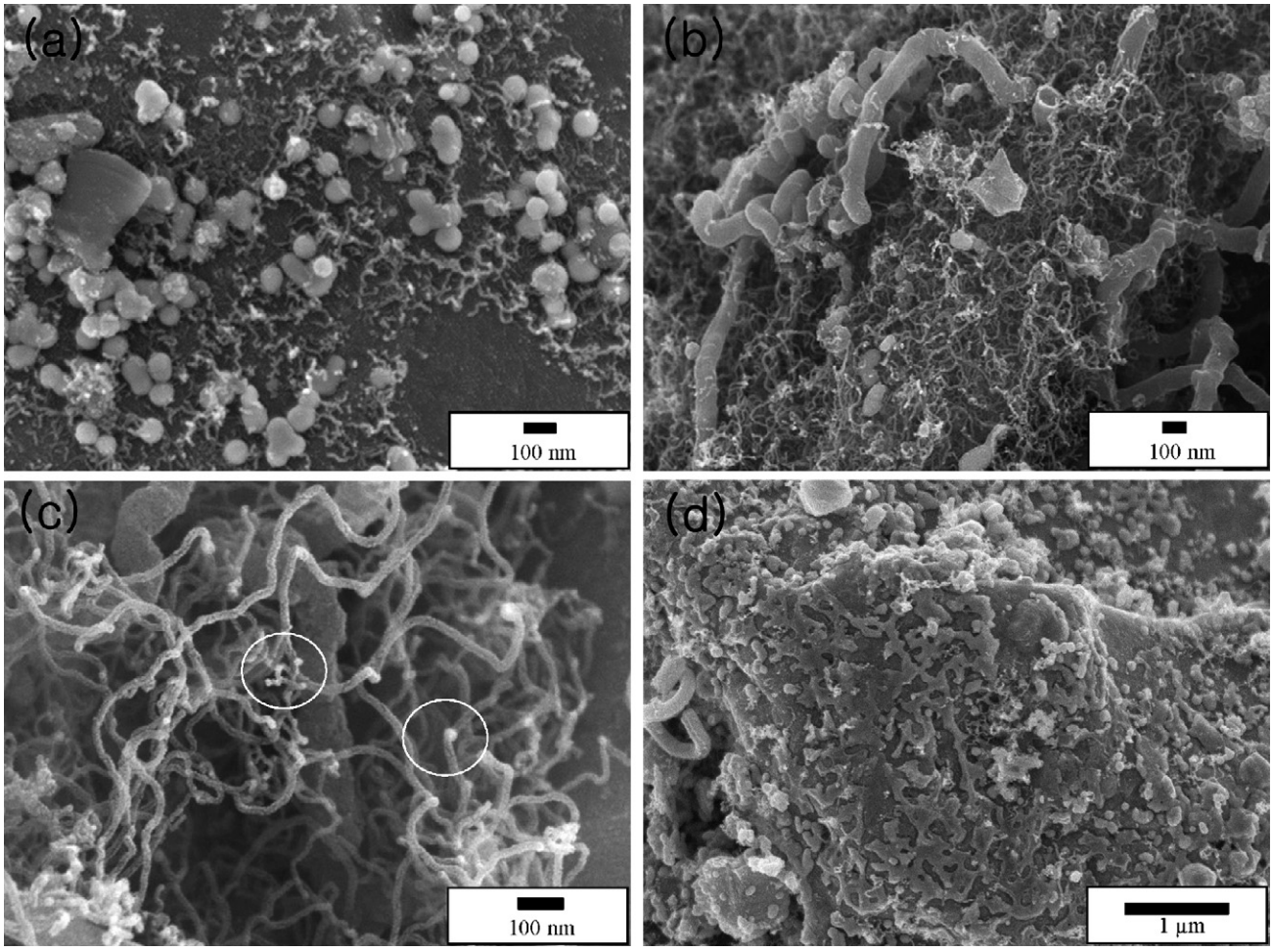

Fig. 2. SEM images of CNTs grown for different periods: (a) 5 min and (b) 30 min. Note CNTs growth takes place preferentially on smaller Ni particles in earlier period. (c) SEM picture that supports tip growth mode, where nickel particles are lifted from the Si surface. (d) SEM image of CNTs grown on Ni-deposited Si particles whose morphology is shown in Fig. 1(c). Note Ni particles were melted and CNTs growth was unsuccessful.

The external morphology of the Si/CNTs composite is shown in Fig. 3(a). The CNTs cover the entire Si surface and the thinner CNTs are dominant. The external morphology clearly shows that the CNTs layer possesses a large amount of void space as the CNTs themselves carry a coiled shape.

3.2. Anodic performance of Si/CNTs composite electrodes

Fig. 4(a) shows galvanostatic charge–discharge voltage curves for the Si/CNTs composite electrode. In the first charging (alloying reaction between Si and Li) curve (the open circles), there appear two main plateaux at 0.8–0.9 V and near 0 V. The absence of the former on the second cycle strongly indicates that this is associated with electrolyte decomposition and concomitant SEI (solid electrolyte interface) formation on the electrode surface [23]. Considering that this type of irreversible capacity is negligible on Si electrode because electrolyte decomposition is not significant on silicon oxides that cover the Si surface [24], the 0.8–0.9 V plateau in Fig. 4(a) can be ascribed to decomposition of electrolyte on the CNTs surface in this composite electrode. This is further confirmed on the charging curve for the pure CNTs electrode shown in the inset, where it is seen that a large amount of irreversible capacity is observed at 0.8–0.9 V. The profiles in the inset also illustrate that the reversible capacity of CNTs is less than 400 mAh g^{-1}, from which it can be inferred that most of the reversible charging and discharging capacity delivered by the Si/CNTs composite electrode is contributed by the Si component itself. Note that the carbon content in this composite is 35.9 wt.%. In addition, the near 0 V charging and 0.45 V discharging shown in Fig. 4(a) is that expected for Si negative electrodes [7–10].

The cycle performance of the Si/CNTs composite electrode is compared with that observed for the bare Si and for the Si/CNTs mixture electrodes (Fig. 4(b)). In the case of the bare Si electrode, the columbic efficiency and cycle performance are the poorest among those for the three types of electrode. The inferior performance of the Si/CNTs mixture electrode compared with that of the composite electrode strongly suggests that composite formation is more advantageous than simple mixing. This is illustrated schematically in Fig. 5. Si powder electrodes are commonly prepared by coating a slurry mixture of Si powder, carbon black and polymeric binder on copper foil. As explained in Section 1, the electric conductive network is vulnerable to breakage during cell cycling. In the case of a normal Si elec-

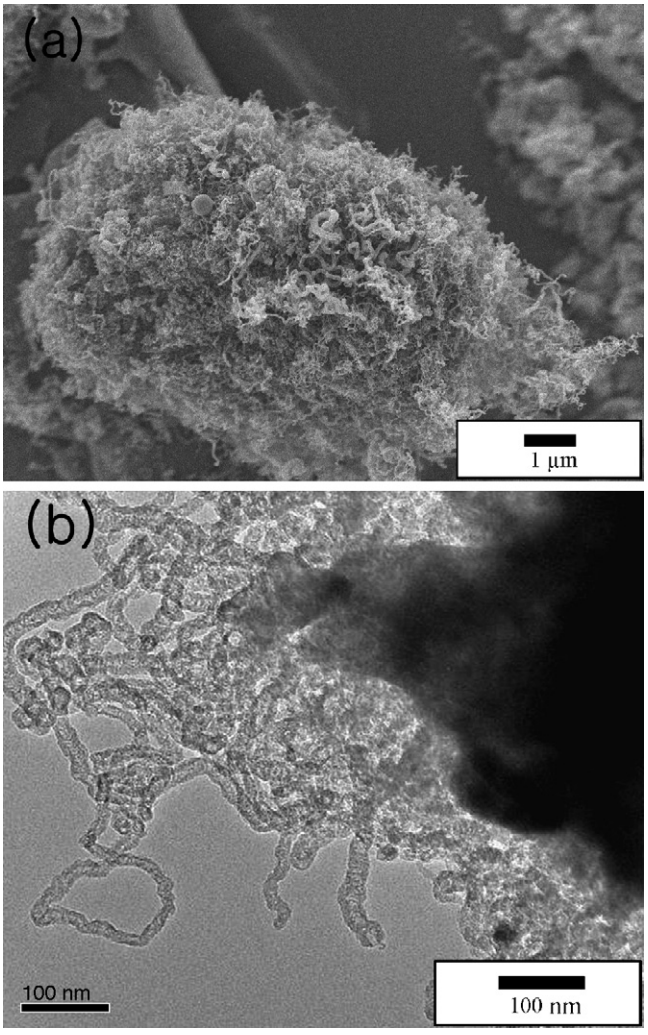

Fig. 3. (a) External morphology (SEM) of Si/CNTs composite and (b) its TEM image. Note coiled CNTs cover entire Si surface and cage-like CNTs layer possesses large amount of void space. Composition of this successfully grown sample was Si:Ni:carbon = 58.4:5.7:35.9 in wt.%.

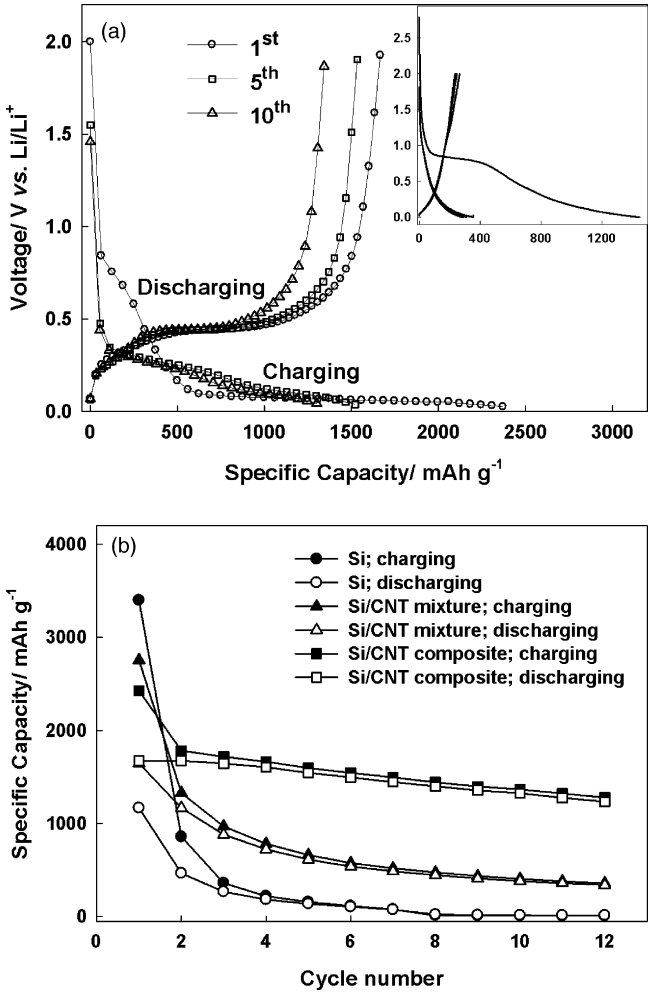

Fig. 4. (a) Galvanostatic charge–discharge voltage curves for Si/CNTs composite electrode. Profile of pure CNTs electrode also presented in inset. (b) Cycle performance of Si/CNTs composite electrode compared with those for bare Si and Si/CNTs mixed electrodes. Note Si/CNTs composite electrode shows best performance.

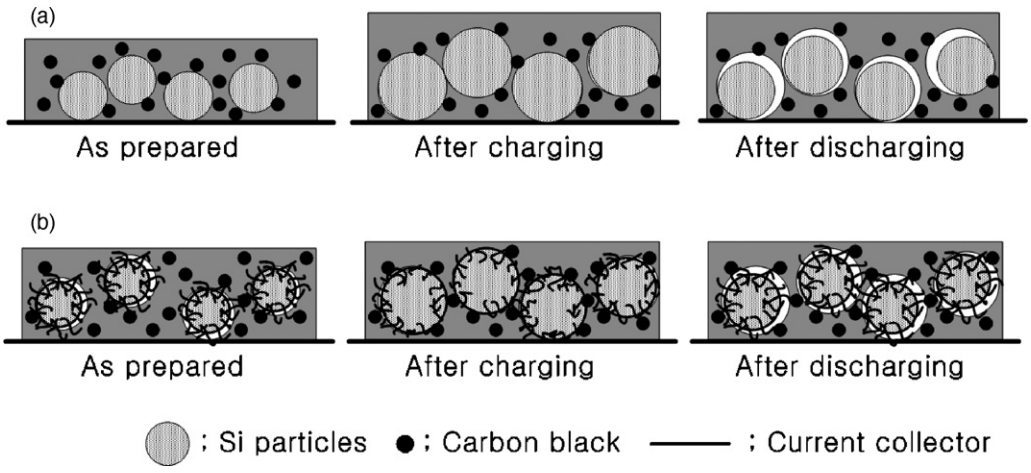

Fig. 5. Schematic illustration of failure mode encountered in Si negative electrode: (a) normal Si and (b) Si/CNTs composite electrode. The breakdown of electronic conductive network, which is severe in (a), is greatly alleviated by buffering action of CNTs, which is due to void space in CNTs layer and mechanical flexibility.

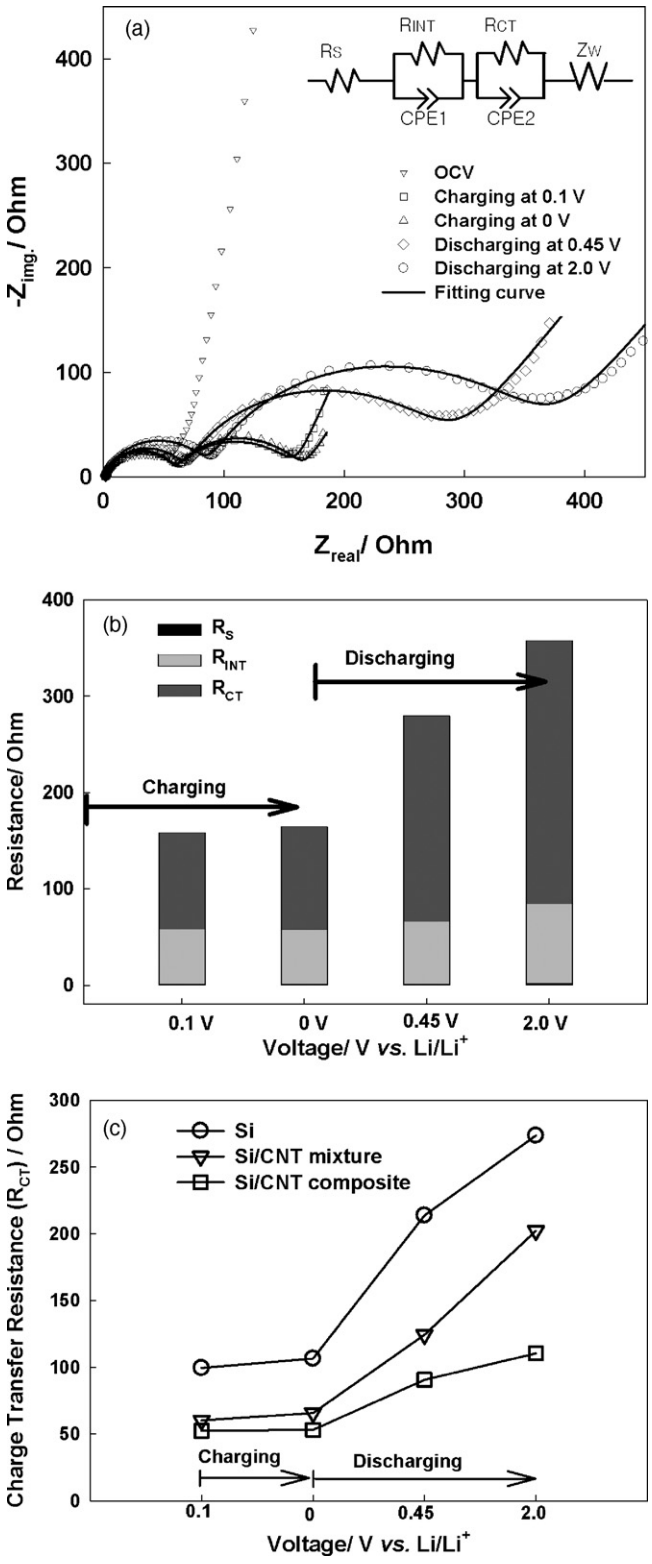

Fig. 6. (a) Nyquist plots recorded with bare Si electrode as function of applied voltage. Equivalent circuit used for curve-fitting presented in inset. (b) Evolution of three resistance components with charge–discharge cycling. Note an abrupt increase in charge-transfer resistance (R_{CT}) during discharging (de-alloying). (c) Variation of R_{CT} for three electrodes. Note R_{CT} enlargement is minimal for Si/CNTs composite electrode and is suggestive of less significant breakdown of conductive network.

trode, this undesirable feature is serious, as depicted in Fig. 5(a). The situation is not much better in the Si/CNTs mixture electrode because the CNTs play the same role as carbon black. In the case of the Si/CNTs composite, however, electrode swelling may not be so severe since the coiled CNTs layer already possesses a void space in the electrode preparation stage.

This void space plays as a buffer against the volume expansion of Si particles during the charging period. Even if the Si particles are contracted in the forthcoming discharging period, the flexible CNTs can still provide an electronic pathway by being stretched. This desirable feature must be possible because the CNTs cover the Si particles as a core/shell, and they are conductive and flexible.

In order to ascertain the buffering action of CNTs, the internal resistance of the Si/CNTs composite electrode was monitored with cycling. Fig. 6(a) presents the a.c. impedance spectra that were recorded for the bare Si electrode. The equivalent circuit used for curve-fitting is provided in the inset. Here, R_S is the resistance associated with the electrolyte and cell component, R_{INT} is the interface resistance relevant to any surface film or silicon oxide layer, R_{CT} is the charge-transfer resistance for the electrode reaction, and Z_W is the Warburg contribution that is related to Li^+ ion diffusion into Si matrix [25]. Two depressed semicircles are suggestive of the porous nature of the electrode and surface non-homogeneity, thereby the capacitor component was replaced by the constant phase element (CPE) in this work [26]. Three resistance components that were derived from the curve-fitting are compared as a function of applied voltage in Fig. 6(b). Both R_S and R_{INT} are largely invariant with respect to the applied voltage, as expected. The R_{CT}, however, shows a potential-dependent behaviour as the charge-transfer rate is potential-dependent. When the applied potential moves in a negative direction from 0.1 to 0.0 V, R_{CT} shows a negligible change within experimental error. Note that a slight decrease is expected since a better electric contact is likely as a result of volume expansion in the Si particles [6]. A rather drastic increase in R_{CT} is observed during the discharge period, which must be a direct result of the loss of electronic paths that is in turn caused by the volume contraction of the Si particles. The potential-dependent R_{CT} is compared for three electrodes in Fig. 6(c). All three electrodes exhibit a negligible variation in R_{CT} during the charging period, but there is a substantial change during the discharging process. Among the three, however, the bare Si electrode exhibits the most significant increase in R_{CT}, and the Si/CNTs composite electrode the least. In the former electrode, therefore, swelling and concomitant loss of electrical contact appear to be the most serious. In the case of the composite electrode, however, this unfavorable feature is greatly suppressed due to the buffering action of the CNTs layer.

4. Conclusion

In this work, CNTs are exploited as a conductive buffer layer to alleviate breakdown of the conductive network in Si negative electrodes. Several meaningful observations have been made, as follows:

(i) Two different types of Ni deposits are generated on the Si surface by the electroless deposition process, namely, spherical grains of several tens of nanometers in diameter and the smaller ones that are thinly deposited to give a film-like external view. CNTs growth is catalyzed preferentially by the smaller Ni deposits. CNTs growth is unsuccessful on larger and thicker Ni deposits, which implies that the size of Ni deposits should be smaller than a certain critical value. The tip growth mode prevails on the Ni/Si surface. In the successfully grown sample, the coiled CNTs layer covers the whole surface of the Si particles to give a cage-like or core/shell type external morphology.

(ii) The electrochemical performance of the Si/CNTs composite electrode has been compared with those of bare Si and Si/CNTs mixed electrodes. Among the three, the composite electrode delivers the best performance. This must be attributed to the conductive buffering role of the CNTs layer. Presumably, the void space in the CNTs layer accepts the volume expansion of core Si particles to minimize the electrode swelling. As a result, the electrical conductive network is maintained even after a volume change in the Si particles. This beneficial feature is confirmed by impedance spectroscopy analysis that showed the enlargement of charge-transfer resistance on discharge to be minimal in the composite electrode. Further work is needed as to determine whether or not the electrode swelling is indeed alleviated in the Si/CNTs composite electrode, which may be possible by using an electrochemical dilatometer.

Acknowledgements

This work was supported by KOSEF via the Research Center for Energy Conversion and Storage, and by the Division of Advanced Batteries in NGE Program (Project no. 10016439).

References

[1] J.O. Besenhard, J. Yang, M. Winter, J. Power Sources 68 (1997) 87.
[2] M. Winter, J.O. Besenhard, Electrochim. Acta 45 (1999) 31.
[3] M. Winter, J.O. Besenhard, M.E. Spahr, P. Novak, Adv. Mater. 10 (1998) 725.
[4] M.N. Obrovac, L. Christensen, Electrochem. Solid State Lett. 7 (2004) A93.
[5] T.D. Hatchard, J.R. Dahn, J. Electrochem. Soc. 151 (2004) A838.
[6] L.Y. Beaulieu, K.W. Eberman, R.L. Turner, L.J. Krause, J.R. Dahn, Electrochem. Solid State Lett. 4 (2001) A137.
[7] M. Yoshio, H. Wang, K. Fukuda, T. Umeno, N. Dimov, Z. Ogumi, J. Electrochem. Soc. 149 (2002) A1598.
[8] N. Dimov, K. Fukuda, T. Umeno, S. Kugino, M. Yoshio, J. Power Sources 147 (2005) 227.
[9] J.W. Kim, J.H. Ryu, K.T. Lee, S.M. Oh, J. Power Sources 114 (2003) 88.
[10] J.H. Ryu, J.W. Kim, Y.E. Sung, S.M. Oh, Electrochem. Solid State Lett. 7 (2004) A306.
[11] W.R. Liu, M.H. Yang, H.C. Wu, S.M. Chiao, N.L. Wu, Electrochem. Solid State Lett. 8 (2005) A100.
[12] Y. Liu, T. Matsumura, N. Imanishi, A. Hirano, T. Ichikawa, Y. Takeda, Electrochem. Solid State Lett. 8 (2005) A599.
[13] Z.P. Guo, E. Milin, J.Z. Wang, J. Chen, H.K. Liu, J. Electrochem. Soc. 152 (2005) A2211.
[14] T. Kim, Y.H. Mo, K.S. Nahm, S.M. S Oh, Proceedings of the 207th ECS Meeting, Quebec City, Canada May 15–20, 2005, Abstract 163.
[15] J. Shu, H. Li, R. Yang, Y. Shi, X. Huang, Electrochem. Commun. 8 (2005) 51.
[16] N. Takano, N. Hosoda, T. Yamada, T. Osaka, J. Electrochem. Soc. 146 (1999) 1407.
[17] H. Ashassi-Sorkhabi, H. Dolati, N. Parvini-Ahmadi, J. Manzoori, Appl. Surf. Sci. 185 (2000) 155.
[18] N. Takano, N. Hosoda, T. Yamada, T. Osaka, Electrochim. Acta 44 (1999) 3743.
[19] V.I. Merkulov, D.H. Lowndes, Y.Y. Wei, G. Eres, Appl. Phys. Lett. 76 (2000) 3555.
[20] Y. Li, W. Kim, Y. Zhang, M. Rolandi, D. Wang, H. Dai, J. Phys. Chem. B 105 (2001) 11424.
[21] C.L. Cheung, A. Kurtz, H. Park, C.M. Lieber, J. Phys. Chem. B 106 (2002) 2429.
[22] A.K.M. Fazle, Y.H. Mo, K.S. Mahm, M.J. Kim, Carbon 40 (2002) 1241.
[23] A.S. Claye, J.E. Fischer, C.B. Huffman, A.G. Rinzler, R.E. Smalley, J. Electrochem. Soc. 147 (2000) 2845.
[24] J.B. Kim, H.Y. Lee, K.S. Lee, S.H. Lim, S.M. Lee, Electrochem. Commun. 5 (2003) 544.
[25] K.M. Shaju, G.V.S. Rao, B.V.R. Chowdari, Electrochim. Acta 48 (2003) 2691.
[26] D. Aurbach, M.D. Levi, E. Levi, H. Teller, B. Markovsky, G. Salitra, J. Electrochem. Soc. 145 (1998) 3024.